Atmos. Meas. Tech. Discuss., 4, 6387–6410, 2011
www.atmos-meas-tech-discuss.net/4/6387/2011/
doi:10.5194/amtd-4-6387-2011

Atmospheric Measurement Techniques Discussions

Tracking of urban aerosols using combined lidar-based remote sensing and ground-based measurements

T.-Y. He[1], S. Stanič[1], F. Gao[1], K. Bergant[1,2], D. Veberič[1], X.-Q. Song[3], and A. Dolžan[4]

[1]University of Nova Gorica, Nova Gorica, Slovenia
[2]Slovenian Environment Agency, Ljubljana, Slovenia
[3]Ocean University of China, Qingdao, China
[4]Optotek d.o.o., Ljubljana, Slovenia

Received: 30 September 2011 – Accepted: 9 October 2011 – Published: 20 October 2011

Correspondence to: T.-Y. He (tingyao.he@ung.si)

Published by Copernicus Publications on behalf of the European Geosciences Union.

Abstract

A measuring campaign was performed over the neighboring towns of Nova Gorica in Slovenia and Gorizia in Italy on 24 and 25 May 2010, to investigate the concentration and distribution of urban aerosols. Tracking of two-dimensional spatial and temporal aerosol distributions was performed using scanning elastic lidar operating at 1064 nm. In addition, PM_{10} concentrations of particles, NO_x and meteorological data were continuously monitored within the lidar scanning region. Based on the collected data, we investigated the flow dynamics and the aerosol concentrations within the lower troposphere and an evidence for daily aerosol cycles. We observed a number of cases with spatially localized increased lidar returns, which were found to be due to the presence of point sources of particulate matter. Daily aerosol concentration cycles were also clearly visible with a peak in aerosol concentration during the morning rush hours and daily maximum at around 17:00 Central European Time. We also found that the averaged horizontal atmospheric extinction within the scanning region 200 m above the ground is correlated to the PM_{10} concentration at the ground level with a correlation coefficient of 0.64, which may be due to relatively quiet meteorological conditions and basin-like terrain configuration.

1 Introduction

It is well known that the presence of particulate matter in the air strongly influences tropospheric chemistry and physics (Braslau and Dave, 1973; Harshvardhan, 1993). With the increasing urbanization and industrialization, high concentrations of particulate matter which are often found in urban areas (Twomey et al., 1978; Hofmann, 1993) are as a rule due to a combination of many aerosol emissions, atmospheric conditions and specific topography of the area. The main increase of aerosol concentrations arises from human activities, which may have significant environmental and climatological impacts as well as considerable effects on human health, as they may e.g. increase

AMTD
4, 6387–6410, 2011

the rates of the atmospheric opto-chemical reactions, reduce visibility and cause epidemiological diseases in general. The guidelines for the ambient air quality in Europe are set by the 2008/50/EC (Directives, 2008) of the European Commission, where the allowed upper limit of PM_{10} particles is set to 50 $\mu g\,m^{-3}$ from 1 January 2010 and the allowed upper limit of $PM_{2.5}$ particles to 25 $\mu g\,m^{-3}$ from 1 January 2015. The need for meeting and enforcing these standards calls for extensive air quality monitoring in inhabited areas.

Basic tools for the assessment of air quality are ground-based monitoring stations that provide continuous point-source measurements of particulate matter concentrations, presence of various gaseous pollutants and general meteorological data. A modern remote sensing tool for the study of atmospheric aerosols is lidar (Measures, 1984; Grant, 1987; Killinger and Menyuk, 1987). Its current uses include the detection of particulate clouds or layers and their mapping, as well as use in air pollution studies, e.g. in the urban boundary layer (e.g. Cooper and Eichinger, 1994; Devara et al., 1994; Menut et al., 1997). Traditional micro pulse lidars (Spinhirne, 1993) are inexpensive and reliable, however, they do not provide high temporal resolution and are not suitable for scanning which is needed for two dimensional aerosol information acquisition. Using scanning lidar (Spuler and Mayor, 2005; Gao et al., 2011) for aerosol tracking and source identification studies becomes more important associated with the emissions.

On 24 and 25 May 2010 we performed a lidar monitoring campaign over the neighboring towns of Nova Gorica in Slovenia and Gorizia in Italy (45.96° N, 13.64° E, 107 m a.s.l.[1]) with the aim of tracking distributions of increased urban aerosol loading and investigating aerosol emissions. The dispersal and the trajectories of potentially hazardous pollutants were obtained from two-dimensional scanning lidar data on atmospheric properties with temporal resolution of about 8 min. Lidar results were complemented by ground-based measurements of PM_{10} and NO_x concentration levels and measurements of local meteorological conditions.

[1] a.s.l. stands for "above sea level".

AMTD
4, 6387–6410, 2011

2 Experimental setup

The cities of Nova Gorica and Gorizia, where the campaign was performed, are located in a basin at the confluence of the Soča (Isonzo) and Vipava Valleys. From the north, they are sheltered from the direct influence of the alpine climate by an intermediate mountain range, from the west by the Goriška Brda (Collio) hills and from the south-eastern by the high Karst plateau, and are thus protected against the cold Bora wind which affects most of the neighboring areas in the Slovenian littoral (Alpers et al., 2007), retaining mild Mediterranean climate throughout the year. In a typical anticyclonic situation, which was present during the campaign, there are generally mild breezes from E-NE in the nighttime and comparatively stronger winds in the daytime from the Adriatic sea in the SW, which is about 20 km away. In an environment with very scarce precipitation from spring to late autumn (Gasith and Resh, 1999), presence of day-night wind reversal and basin-like terrain configuration the risk of increased aerosol loading in urban settings is expected to be high, which calls for a systematic monitoring effort for quantitative estimation of concentration levels as well as spatial and temporal variability of aerosols. The present monitoring campaign was the first attempt in Slovenia to address this problem using a combination of remote sensing and ground-based monitoring.

2.1 Remote sensing

Remote sensing was performed using a bi-axial scanning mobile lidar. The device was designed for day- and night-time studies of tropospheric conditions (He et al., 2010) and provides automatic scanning in both azimuth and elevation angle with an angular resolution of 0.1°. The lidar was set up at an elevated site northeast from Nova Gorica (305 m a.s.l., 200 m above the basin ground) with clear horizontal visibility over the entire region of interest (Fig. 1). A pulsed Nd:YAG Laser[2] was used as the

[2]Big Sky CFR400 by Quantel, France

AMTD
4, 6387–6410, 2011

transmitter, providing 8 ns width pulses with a maximum repetition rate of 10 Hz at 266 and 1064 nm. In this study only the infrared channel was used to minimize the amount of molecular scattering compared to scattering on particles. The pulse energy was set to 40 mJ in order to prevent saturation of the receiver in the near field. Backscattered light was collected by a Newtonian telescope with a diameter of 300 mm. To suppress the background in daytime operation, an adjustable iris was placed at the focus of the telescope and a 1 nm interference filter[3] centered at 1064 nm was used. The signal was detected by an avalanche photodiode (APD)[4]. Data acquisition was performed using a Licel transient recorder[5] with 12-bit resolution at 40 MHz sampling rate in combination with C++ (Linux) based own data acquisition software. These digitization parameters yield a range resolution of 3.75 m and a maximum detection range of 61.4 km.

To observe two-dimensional temporal and spatial distribution of aerosols, two scan patterns were executed, Range Height Indicator (RHI) scan and Plane Position Indicator (PPI) scan. In RHI scan, the elevation angle was increased in 1° steps from 4° to 45° (covering a range of 41°) at a constant azimuth angle of 230°. In PPI scan the elevation angle was set to zero and the azimuth angle was changed in 2° steps in counter-clockwise direction from 267° to 205° covering a range of 62°. At each step, 150 laser shots were averaged and each scan took approximately 8 min to complete.

2.2 Ground-based measurements

Due to the elevated risk of increased aerosol loading in Nova Gorica region, the concentration of PM_{10} particles is being continuously monitored by the Slovenian Environment Agency. The monitoring site is located within the scanning area in a vicinity of a frequented road in Nova Gorica (Fig. 1). True mass concentrations were provided by

[3]Barr Associates Inc., USA
[4]EG&G C30954/5E, URS Corporation, USA
[5]TR40-160 transient recorder, Licel, Germany

AMTD
4, 6387–6410, 2011

an ambient particulate monitor[6] positioned 2 m above the ground. In addition, NO_x and meteorological data (wind speed and direction 10 m above the ground, temperature and relative humidity 2 m above the ground) were also collected at the same site. All ground-based data were averaged every hour except for the wind speed and direction, which were averaged every half an hour.

3 Analysis of lidar data

The lidar return signal along a single line of sight can be modeled (Collis and Russel, 1976) as

$$P(r) = \frac{kE_0\beta(r)}{r^2}\exp\left[-2\int_0^r \alpha(r')\mathrm{d}r'\right], \quad (1)$$

where $P(r)$ is the received signal, k the lidar system constant including the losses in the transmitting and receiving optics and the effective receiver aperture, E_0 the laser pulse energy, β the volume backscatter ($m^{-1}\,sr^{-1}$), and α the extinction coefficient (m^{-1}). Raw data was normalized to the laser energy and the flat baseline of each return, which is proportional to the intensity of background noise, was subtracted. Background noise was defined as an average of data points sampled at the far end of the trace. Each lidar return was then corrected for inverse-range-squared dependence (Measures, 1988). To improve the signal-to-noise ratio, a five-point gliding type radial basis spatial filter algorithm with weights given by Pascal's triangle was employed. Maximum detectable range with signal-to-noise ratio larger than one was then found to be about 5 km. Spatial distribution of the range-corrected lidar return signal obtained by both RHI and PPI scanning was presented by Cartesian 2-D scans. To fill the pixels where no lidar data was available, a weighted value was reconstructed using a barycentric interpolation scheme (Min, 2004) between successive step profiles.

[6]TEOM series 1400a ambient particulate monitor, Thermo Electron Corporation, USA

AMTD
4, 6387–6410, 2011

To be able to normalize lidar return signals to aerosol concentrations they need to be transformed into atmospheric extinction profiles. In urban areas, Klett solution (Klett, 1981) of the vertical extinction profile can be highly erroneous because of the relatively large uncertainty of the lidar ratio. The multiangle method (Kano, 1968; Hamilton, 1969; Filipčič et al., 2003) is a possible way to obtain vertical extinction profiles from different elevation angle data obtained with scanning lidar under the assumption of horizontal atmospheric homogeneity and without the need to select specific lidar ratio. As the atmospheric boundary layer over urban areas is generally turbulent and heterogeneous (Spinhirne et al., 1980; Kovalev and Eichinger, 2004), this method is rarely used due to the inaccuracy of the horizontal atmospheric homogeneity assumption along any single trace. However, as aerosol fluctuations in horizontal directions are mostly random, lidar return data averaged over the entire horizontal scan does allow for a relatively accurate calculation of spatially averaged aerosol extinction at specific height.

As the lidar operated in the infrared part of the spectrum, the contribution from molecular scattering to extinction and backscatter coefficients was considered to be negligible. Effects of atmospheric inhomogeneities on the aerosol extinction coefficient α (which may be caused by localized pollution sources and meteorological conditions) were minimized by using the average of the lidar S-function,

$$\bar{S}(r) = \left\langle \ln\left[r^2(P(r) - P_{\mathrm{bg}})\right] \right\rangle = \ln(k\beta) - 2\alpha r\,, \tag{2}$$

over each horizontal PPI scan in the deconvolution process. In the averaging, directions with apparent nonlinear data (e.g. with the presence of point sources) were excluded. Horizontal atmospheric extinction coefficient was obtained using the slope method (Collis, 1966) as the slope of the least-squares straight line fit to $\bar{S}(r)$ through the considered range (Fig. 4). The deviations of atmospheric extinction coefficient α from linearity are a suitable criterion for the detection of the extent of horizontal heterogeneity of the atmosphere and thus can be used as an estimator for the quality of the retrieved data.

AMTD
4, 6387–6410, 2011

The total uncertainty related to the lidar-based measurement of aerosol extinction coefficient arose from three major sources, the uncertainty of the system constant factor k, the error in the background subtraction, and the horizontal atmospheric inhomogeneity (Eq. 2). The contribution of the system constant uncertainty for the case of thermally stabilized lidar return detection system is typically less than 0.05 (e.g. PerkinElmer, 2011). Relative uncertainty arising from background subtraction is related to the signal-to-noise ratio of the lidar system. As the lidar signal decreases with distance as $1/r^2$ (Eq. 1), this uncertainty tends to be smaller closer to the lidar site and greater further away from the lidar. In our case, the deviation of background noise was 0.12 mV out of approximately 5 mV at the range of 3.5 km. The uncertainty from background noise subtraction was on the average found to be 0.03. Dominant contribution to the total uncertainty of the measurement was due to horizontal atmospheric inhomogeneities. These were estimated by considering the nonlinearity of the lidar S-function signal $S(r)$ for horizontal traces with different azimuth angles at a fixed distance from the lidar site (e.g. azimuthal nonlinearity) and the nonlinearity of the averaged S-function signal $\bar{S}(r)$ within the considered range, where the apparently nonlinear data (less than 10 % of the full scan) were excluded from the calculation. The upper limit on azimuthal nonlinearities were calculated at the distance of 3.5 km from the lidar site, which was chosen to maximize the effects of heterogeneity due to geometrical distance between successive azimuthal profiles. Relative uncertainty due to horizontal inhomogeneity was estimated to be less than 0.2. These three uncertainties are assumed to be statistically independent, a total relative uncertainty of aerosol extinction coefficient was estimated to be less than 0.21.

4 Results and discussion

Using the lidar data from the campaign and the standard ground-based monitoring data, several case studies were performed, including the observation of the vertical structure dynamics in the lower troposphere, the identification of aerosol point sources

AMTD
4, 6387–6410, 2011

and the study of daily aerosol cycles. In addition, a correlation study between the lidar-based and ground-based data was also performed.

4.1 Structure of the lower troposphere

In the daytime and under unstable, windy conditions the lower troposphere is usually well mixed due to the convection or vertical wind shear. On the other hand, in stable atmospheric conditions some horizontally stratified layers can be formed, especially during the night. In our case study we used RHI scans to reveal vertical distribution of aerosols in the lower troposphere. The main purpose of the case study was to investigate the transition from the horizontally stratified lower troposphere formed during the night to well mixed lower troposphere due to the increased thermal convection during the daytime. An example of temporal development of vertical structure of the lower troposphere, illustrated by a series of RHI scans performed from 11:00 to 12:30 CET[7] on 24 May 2010, is shown in Fig. 2. At 11:03 CET, lower troposphere was still horizontally stratified (Fig. 2a) and several optically-thin aerosol layers can be seen up to the 1.6 km above the lidar site. At the height of about 2 km a layer of low level clouds was also present. In the next one and a half hour (Fig. 2b–d), increased solar radiation caused the low clouds to slowly diminish and therefore more solar radiation reached the surface. Solar heating of the surface and consequential heating of the air at the surface intensified thermal convection and mixing of the air in the lower troposphere, which caused the degradation of the stratified layers. The effect of the heating was additionally confirmed by an evident increase of air temperature and the increase in wind speed (Fig. 3) in the period between 11:00 and 12:30 CET. The described turbulent atmospheric conditions due to changing structure of the lower troposphere were the main source of uncertainty in the horizontal aerosol extinction coefficient used to correlate remote sensing with ground based measurements.

[7] All times in this paper refer to Central European Time (CET).

AMTD
4, 6387–6410, 2011

4.2 Identification of aerosol sources

In urban areas, main aerosol sources are expected to be localized exhausts from industrial and domestic emissions and traffic along the roadways. Individual aerosol emissions can not be distinctly visible in the single-point ground based PM_{10} and NO_x monitoring data because of spatial and temporal averaging, however, time-series of the remote sensing scanning data can reveal the exact locations of the sources and complex dispersion paths of the plumes. We attempted to identify aerosol sources from the spatial distribution of the range-corrected lidar return signal in the horizontal PPI scans.

During the lidar campaign, a total of 8 distinct cases of localized increases of lidar return were observed, all of them in the industrial area in north-west of Nova Gorica. Using the range and azimuth information from horizontal PPI scans, these cases were found appear at four different locations (Fig. 1) with polar coordinates of A = [1.7 km, 265°], B = [1.55 km, 262°], C = [1.7 km, 258°] and D = [1.8 km, 245°] with respect to the lidar site. After visual inspection of these locations in the field, they were confirmed to be major industrial aerosol sources, namely processing plants (A) and (D), lime production plant (B) and a foundry (C). In most cases, the plume emitted from these sources was found to spread towards inhabited areas.

Examples of aerosol emissions from sources (B) and (D) can be seen in horizontal PPI sector scans performed at 09:19 and 11:28 CET on 25 May 2010 (Fig. 5), where both show localized increases of lidar return. In the scan taken at 09:19 CET in calm wind conditions, the increased lidar return was found to be localized above the source (B) only. In the scan at 11:28 CET, the plume from the source (D) was found to be carried in a relatively straight line towards the north-east for about 800 m due to the emerging south-western wind (Fig. 3b), after which it disappeared (either blended in with background aerosols or rose above the scanning plane). Based on the logarithmic velocity law (Garratt, 1992), rapid dispersal of the plume can be explained by the presence of a stronger wind around the lidar scanning height.

AMTD
4, 6387–6410, 2011

4.3 Daily aerosol cycles

In urban areas, aerosol concentration levels were found to be strongly related to human activities, which result in the appearance prominent features in daily aerosol cycles. These cycles are clearly visible in ground-based PM_{10} and NO_x monitoring data (e.g. Harrison et al., 1999). Daily variations of PM_{10} and NO_x in Nova Gorica on 24–25 May 2010 are shown in Fig. 6. The increase in both PM_{10} and NO_x concentration levels peaking at around 8:00 CET was found to present not only on these two days, but as a rule in the long-term data and can be related to the traffic emissions in the morning rush hours. In addition to the exhaust emissions, an amount of road dust was pick-up and injected into the troposphere by vehicles may also be responsible for the concentration increase (e.g. Eichinger et al., 1994). The NO_x concentration had an apparent low in the afternoon, while the PM_{10} increased and reached a plateau at around 17:00 CET. Relatively low and constant concentrations of PM_{10} and NO_x during the night are expected to be the result of significantly reduced traffic and the absence of strong localized night-time sources outside the heating season.

In the lidar monitoring campaign, scanning measurements were performed from 09:00 to 16:00 CET on 24 May 2010 and from 09:00 to 18:00 CET on 25 May 2010. The late morning increase of aerosol concentrations over the entire area is visible from temporal evolution of lidar derived aerosol extinction, obtained from horizontal PPI scans 200 m above the ground (Fig. 7). Despite the fact that aerosol extinction is due to scattering on particulate matter and should therefore follow more or less the same daily pattern, several differences were found. There was a rapid decrease of aerosol concentration at the ground level after 10:00 CET due to the decrease of traffic intensity and the increase of the south-western updraft wind speed (Fig. 3a), which was not observed in the scanning data. We expect this to be due to basin-like terrain configuration so that the aerosols remained contained and were present at the lidar scanning height. The decrease of aerosol extinction between 13:00–16:00 CET was not observed in the PM_{10} measurements, which were more or less constant. In such

AMTD
4, 6387–6410, 2011

a case, we expect the aerosol extinction decrease to be due, at least in part, to the increased water evaporation from hygroscopic aerosols (e.g. Lewandowski et al., 2010) during the daily temperature maximum (Fig. 3c). Another reason for the decrease could be that in this period the convection was the strongest. The resulting mixing of air-masses and the increase of the boundary layer height would decrease aerosol concentrations in the entire Nova Gorica basin, including at the lidar scanning height.

4.4 Correlation between aerosol extinction and PM_{10} concentration

As the aerosol extinction is a result of Mie scattering on particulate matter in the atmosphere, it is expected to be highly correlated to particle concentrations with categories of particular size, such as PM_{10} and $PM_{2.5}$ concentration, which was experimentally confirmed in several studies (e.g. Del Gusta and Marini, 2000; Lagrosas et al., 2005).

In our case study, in the absence of the data regarding the distribution of aerosol size, a simple comparison of horizontal aerosol extinction and PM_{10} concentration was made. The trends of two independent data are in good agreement, with a small offset. The major sources of uncertainties are expected to be the different location of the two measurements – PM_{10} data was collected at the ground level while lidar measurements were performed 200 m above the ground. As relatively quiet meteorological conditions and basin-like terrain configuration, using hourly averaged horizontal atmospheric extinction (α) and PM_{10} concentration (c), the correlation between α_{1064} and c was found to be linear, $\alpha_{1064} = (0.00192 \pm 0.00012)c$ with a correlation coefficient of 0.64 (Fig. 8). In the fit, α was constrained to zero for the limit case when PM_{10} concentration is zero.

5 Conclusions

The case studies of aerosol monitoring performed over the neighboring towns of Nova Gorica in Slovenia and Gorizia in Italy on 24 and 25 May 2010 showed that a combination of remote sensing and in-situ ground measurements provides useful additional

AMTD
4, 6387–6410, 2011

information for the investigation of the effects of urban environment. The sources of uncertainties in the lidar measurements were investigated in detail and the relative error of the aerosol extinction coefficient was found to be less than 0.21.

Regarding the structure of the lower troposphere, complex flow dynamics between layers with increased aerosol content was observed. In the case of identification of aerosol sources, lidar-based remote sensing was found to be essential. Using horizontal PPI plots of the range-corrected lidar return signal four distinct aerosol point sources were identified in the industrial area of Nova Gorica and later confirmed by the inspection in the field. Daily aerosol cycles, routinely observed in ground-based monitoring data were observed in lidar-based data as well, with noticeable differences between the temporal evolution of aerosol extinction and PM_{10} concentration. These differences could be related to the topological properties of the urban region, the properties of the aerosol particles and the daily meteorological conditions. Up to four times higher aerosol concentrations during the rush hours in comparison to the daily average indicate that traffic plays an important role air pollution in the Nova Gorica/Gorizia region. Finally, an attempt was made to correlate the horizontal aerosol extinction obtained from remote sensing to mass concentration, obtained from the measurements of PM_{10} concentration. These two measurements were found to be linearly correlated with a correlation coefficient of 0.64. Maximum aerosol extinction of 0.1 km^{-1} at 1064 nm obtained in the campaign corresponds to about 40 $\mu g\, m^{-3}$.

Acknowledgements. We wish to thank Romina Žabar and Gostilna Kekec for providing the measuring site above Nova Gorica and Tanja Bolte from Slovenian Environment Agency for providing the ground-based data. We also acknowledge the financial support of the Slovenian Research Agency.

AMTD
4, 6387–6410, 2011

References

Alpers, W., Ivanov, A. Y., and Horstmann, J.: Bora events over the Adriatic Sea and Black Sea studied by multi-sensor satellite imagery, in: Proc. International Geoscience and Remote Sensing Symposium (IGARSS), Toulouse, France, 1307–1313, 2007. 6390

Braslau, N. and Dave, J. V.: Effects of aerosols on the transfer of solar energy through realistic atmosphere. Part I: Nonabsorbing aerosols, J. Appl. Meteorol., 12, 610–615, 1973. 6388

Collis, R. T. H.: LIDAR: A new atmospheric probe, Q. J. Roy. Meteorol. Soc., 92, 220–230, 1966. 6393

Collis, R. T. H. and Russel, P. B.: Lidar measurement of particles and gases by elastic backscattering and differential absorption, in: Laser Monitoring of the Atmosphere, edited by: Hinkley, E. D., Springer, Berlin, 71–151, 1976. 6392

Cooper, D. and Eichinger, W.: Structure of the atmosphere in an urban planetary boundary layer from lidar and radiosonde observations, J. Geophys. Res., 99, 22937–22948, 1994. 6389

Del Gusta, M. and Marini, S.: On the retrieval of urban mass concentrations by a 532 and 1064 nm LIDAR, J. Aerosol Sci., 31, 1469–1488, 2000. 6398

Devara, P. C. S., Raj, P. E., and Sharma, S.: Remote sensing of atmospheric aerosol in the nocturnal boundary layer, Environ. Pollut., 85, 97–102, 1994. 6389

Directive 2008/50/EC of the European parliament and of the council of 21 May 2008 on ambient air quality and cleaner air for Europe, Official Journal of the European Union, L152, 30–35, 2008. 6389

Eichinger, W., Cooper, D., Buttler, W., Cottingame, W., and Tellier, L.: Use of lidar for the evaluation of traffic-related urban pollution, Bellingham, WA, Proc. SPIE, 2102, 209, doi:10.1117/12.170636, 1994. 6397

Filipčič, A., Horvat, M., Veberič, D., Zavrtanik, D., and Zavrtanik, M.: Scanning lidar based atmospheric monitoring for fluorescence detectors of cosmic showers, Astropart. Phys., 18, 501–512, 2003. 6393

Gao, F., Bergant, K., Filipčič, A., Forte, B., Hua, D.-X., Song, X.-Q., Stanič, S., Veberič, D., and Zavrtanik, M.: Observations of the atmospheric boundary layer across the land-sea transition zone using a scanning Mie lidar, J. Quant. Spectrosc. Ra., 112, 182–188, 2011. 6389

Garratt, J. R.: The Atmospheric Boundary Layer, Cambridge University Press, Cambridge, UK, 1992. 6396

AMTD
4, 6387–6410, 2011

Gasith, A. and Resh, V. H.: Streams in Mediterranean climate regions: abiotic influences and biotic responses to predictable seasonal events, Annu. Rev. Ecol. Syst., 30, 51–81, 1999. 6390
Grant, W. B.: Laser remote sensing techniques, in: Laser Spectroscopy and its Applications, edited by: Radziemski, L. J., Solarz, R. W., and Paisner, J. A., Marcel Dekker, New York, 1987. 6389
Hamilton, P. M.: Lidar measurement of backscatter and attenuation of atmospheric aerosol, Atmos. Environ., 3, 221–223, 1969. 6393
Harrison, R. M., Jones, M., and Collins, G.: Measurements of the physical properties of particles in the urban atmosphere, Atmos. Environ., 33, 309–321, 1999. 6397
Harshvardhan: Aerosol-Climate interactions, in: Aerosol-Cloud-Climate Interactions, edited by: Hobbs, P. V., Academic Press, San Diego, California, 75–95, 1993. 6388
He, T.-Y., Gao, F., Stanič, S., Veberič, D., Bergant, K., Dolžan, A., and Song, X.-Q.: Scanning mobile lidar for aerosol tracking and biological aerosol identification, Proc. SPIE, 7832, 7832U, doi:10.1117/12.868387, 2010. 6390
Hofmann, D. J.: Twenty years of balloon borne tropospheric aerosol measurements at Laramie, Wyoming, J. Geophys. Res., 98, 12753–12766, 1993. 6388
Kano, M.: On the determination of backscattered and extinction coefficient of the atmosphere by using laser radar, Pap. Meteorol. Geophys., 19, 121–129, 1968. 6393
Killinger, D. K. and Menyuk, N.: Laser remote sensing of the atmosphere, Science, 235, 37–45, doi:10.1126/science.235.4784.37, 1987. 6389
Klett, J. D.: Stable analytical inversion solution for processing lidar returns, Appl. Opt., 20, 211–220, 1981. 6393
Kovalev, V. A. and Eichinger, W. E.: Elastic Lidar: Theory, Practice and Analysis Methods, Wiley and Sons, New York, 2004. 6393
Lagrosas, N., Kuze, H., Takeuchi, N., Fukagawa, S., Bagtasa, G., Yoshii, Y., Naito, S., and Yabuki, M.: Correlation study between suspended particulate matter and portable automated lidar data, Aerosol Sci., 36, 439–454, 2005. 6398
Lewandowski, P. A., Eichinger, W. E., Holder, H., Prueger, J., Wang, J., and Kleinman, L. I.: Vertical distribution of aerosols in the vicinity of Mexico City during MILAGRO-2006 Campaign, Atmos. Chem. Phys., 10, 1017–1030, doi:10.5194/acp-10-1017-2010, 2010. 6398
Measures, R. M.: Laser Remote Sensing: Fundamentals and Applications, Wiley, New York, 1984. 6389

AMTD
4, 6387–6410, 2011

Measures, R. M.: Laser Remote Chemical Analysis, Wiley, New York, 1988. 6392
Menut, L., Flamant, C., Pelon, J., Valentin, R., Flamant, P. H., Dupont, E., and Carissimo, B.: Study of the boundary layer structure over the Paris agglomeration as observed during the ECLAP Experiment, in: Advances in Atmospheric Remote Sensing with Lidar, edited by: Ansmann, A., Neuber, R., Rairoux, P., and Wandinger, U., Springer, Berlin, 15–18, 1997. 6389
Min, C.: Local level set method in high dimension and codimension, J. Comput. Phys., 200, 368–382, 2004. 6392
PerkinElmer Datasheet: Long wavelength Enhanced Silicon APD, C30954EH, C30955EH and C30956EH Series, available at: www.excelitas.com/downloads/DTS_LongWLEnSiliconAPDSeries.pdf, 2011. 6394
Spinhirne, J. D.: Micro pulse lidar, IEEE T. Geosci. Remote Sens., 31, 48–55, 1993. 6389
Spinhirne, J. D., Reagan, J. A., and Herman, B. M.: Vertical distribution of aerosol extinction cross section and inference of aerosol imaginary index in the troposphere by lidar technique, J. Appl. Meteorol., 19, 426–438, 1980. 6393
Spuler, S. M. and Mayer, S. D.: Scanning eye-safe elastic backscatter lidar at 1.5-micron wavelength, J. Atmos. Ocean. Technol., 22, 696–703, 2005. 6389
Twomey, S. A., Davidson, K. A., and Seton, K. J.: Results of 5 years' of observations of cloud nucleus concentrations at Robertson, New South Wales, J. Atmos. Sci., 35, 650–656, 1978. 6388

AMTD
4, 6387–6410, 2011

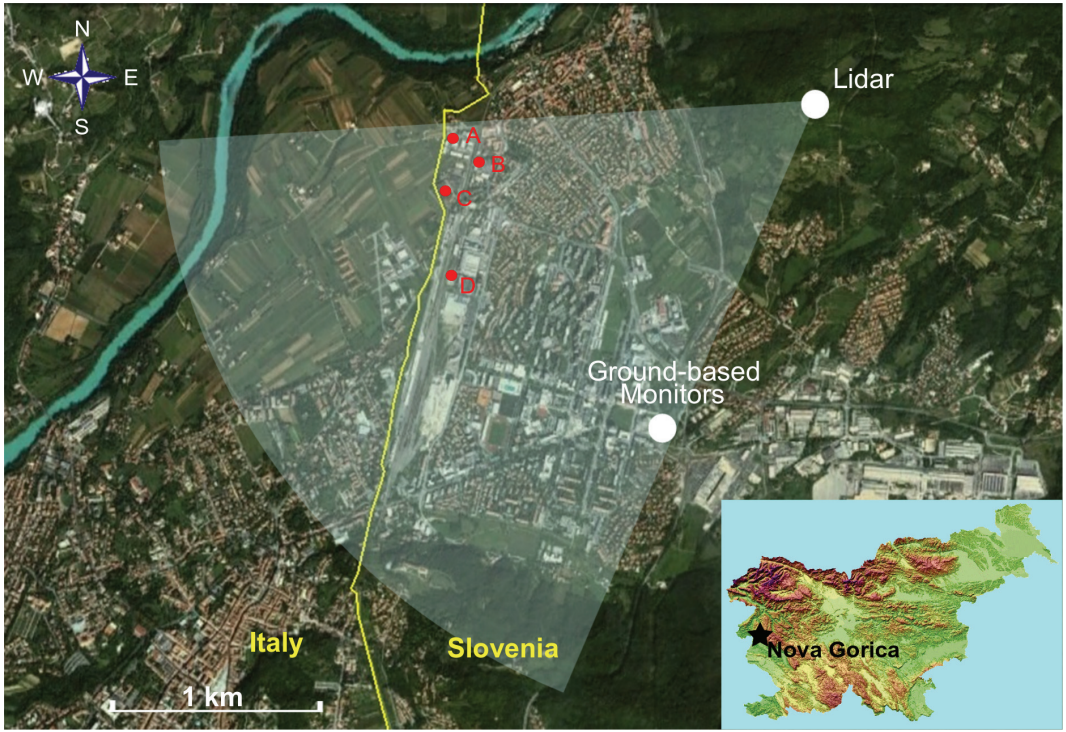

Fig. 1. Top view of the scanning region (white shadow) and the lidar site (45.96° N, 13.64° E, 305 m a.s.l., 200 m above the town). PM_{10}, NO_x and meteorological data were monitored at the ground level. Red points denote the locations of the identified aerosol sources and the yellow line the border between Slovenia and Italy.

AMTD
4, 6387–6410, 2011

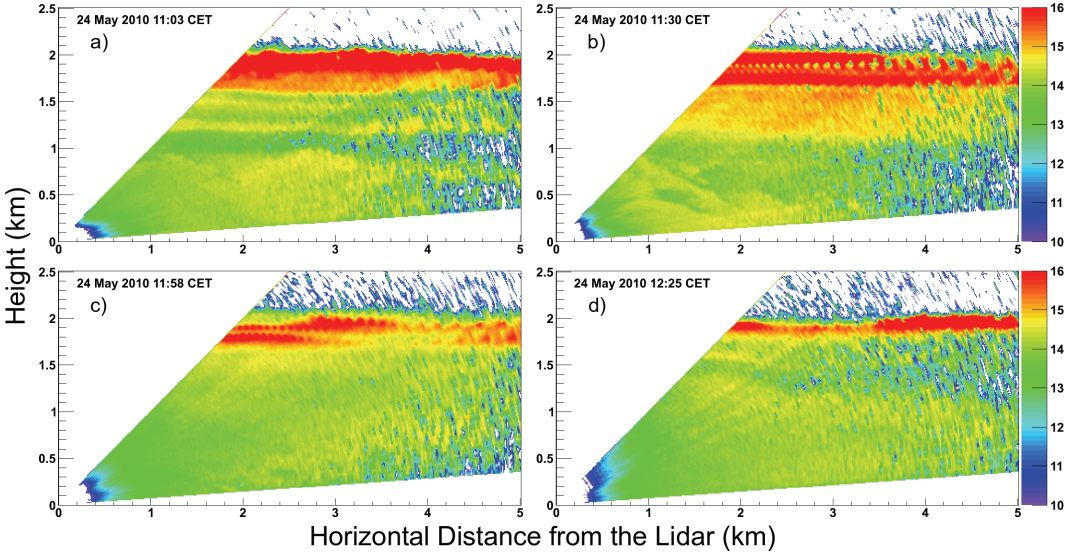

Fig. 2. Time series of vertical RHI scans from 4° to 45° with angular step of 1°, performed from 11:00 through 12:30 CET on 24 May 2010. The presence of a lower layer of clouds can be seen throughout the scanning period at the altitude of 2 km relative to the lidar site. Above 2 km, lidar signal is effectively blocked by the clouds.

AMTD
4, 6387–6410, 2011

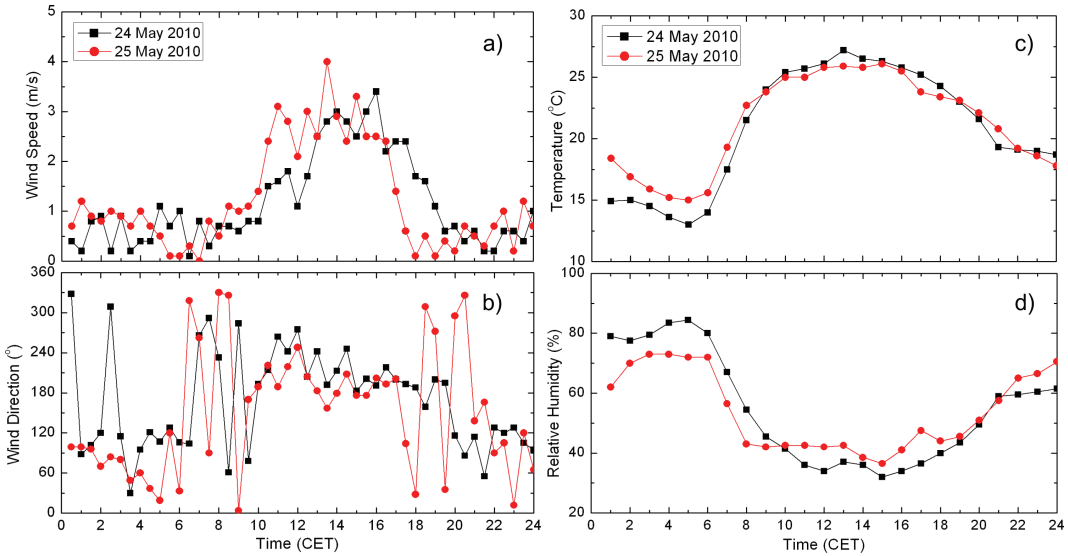

Fig. 3. Meteorological data for Nova Gorica on 24–25 May 2010. Wind information was obtained 10 m above the ground and the temperature and relative humidity 2 m above the ground.

AMTD
4, 6387–6410, 2011

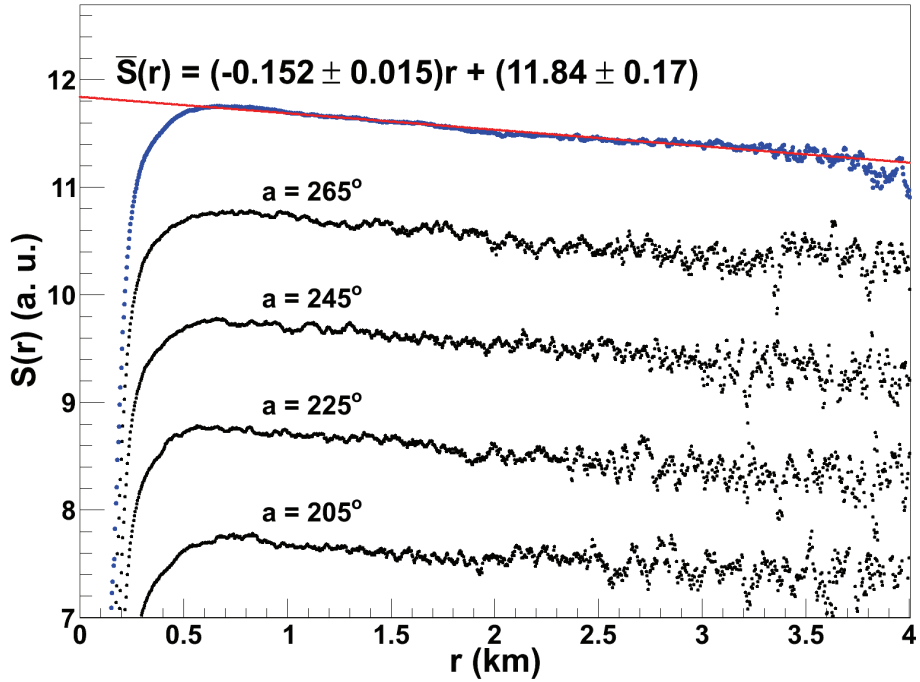

Fig. 4. Averaged S-function for different horizontal directions over the PPI scan performed at 11:54 CET on 25 May 2010, with apparent nonlinear data excluded. The line $\bar{S}(r) = (-0.152 \pm 0.015)r + (11.84 \pm 0.17)$ is a result of least squares linear fit in the range between 0.8 and 3.5 km, yielding a correlation coefficient of 0.94. The resulting horizontal atmospheric extinction coefficient α is 0.076 km^{-1} with relative error of about 0.1 due to atmospheric inhomogeneity. S-functions with azimuthal angles of 265°, 245°, 225°, and 205° are also shown with an incremental shift minus one from the averaged value.

AMTD
4, 6387–6410, 2011

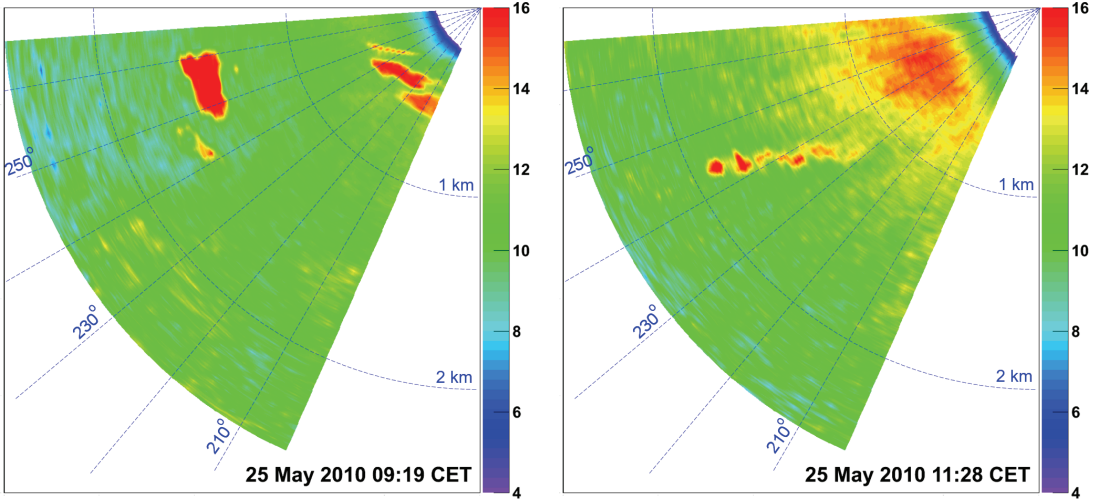

Fig. 5. Two examples of horizontal PPI sector scans performed at 9:19 and 11:28 CET on 25 May 2010 show localized increases of lidar return corresponding to aerosol emission sources (B) and (D). In the later scan, the dispersion of the plume (D) towards the NE due to the increased wind speed can be clearly seen.

AMTD
4, 6387–6410, 2011

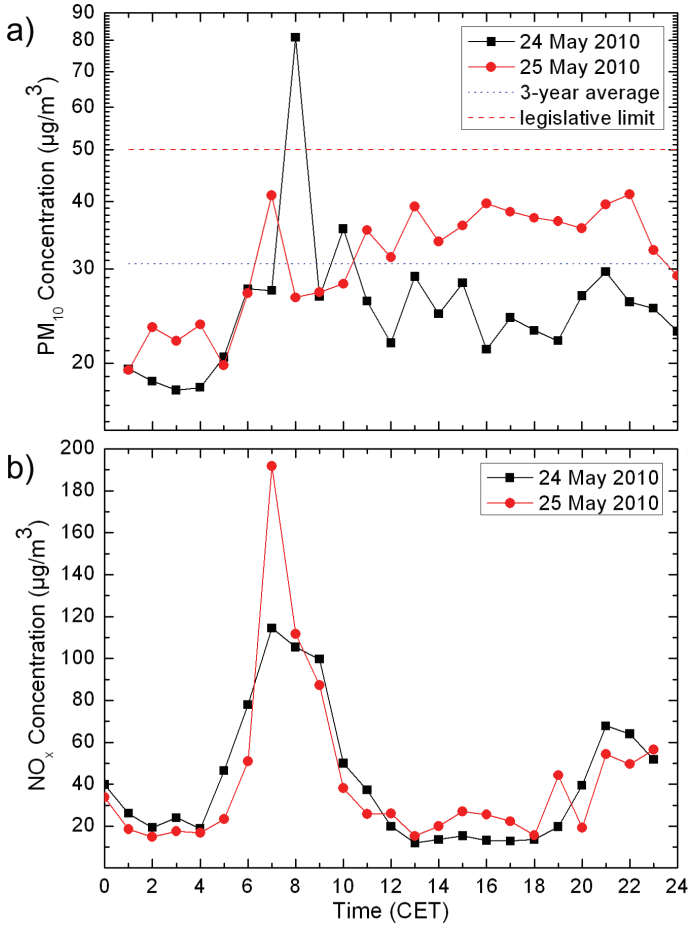

Fig. 6. Temporal evolution of PM_{10} and NO_x concentrations for the period of on 24–25 May 2010, obtained from the ground-based measurements at the monitoring station in Nova Gorica.

AMTD
4, 6387–6410, 2011

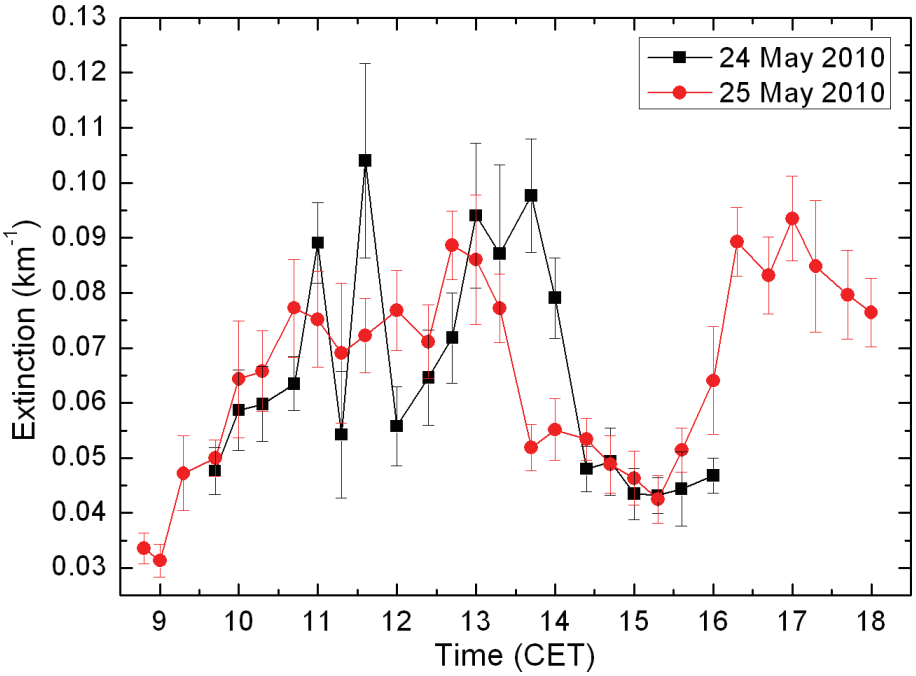

Fig. 7. Temporal evolution of lidar derived aerosol extinction coefficients 200 m above the town from 9:00 to 16:00 CET on 24 May 2010 and from 9:00 to 18:00 CET on 25 May 2010.

AMTD
4, 6387–6410, 2011

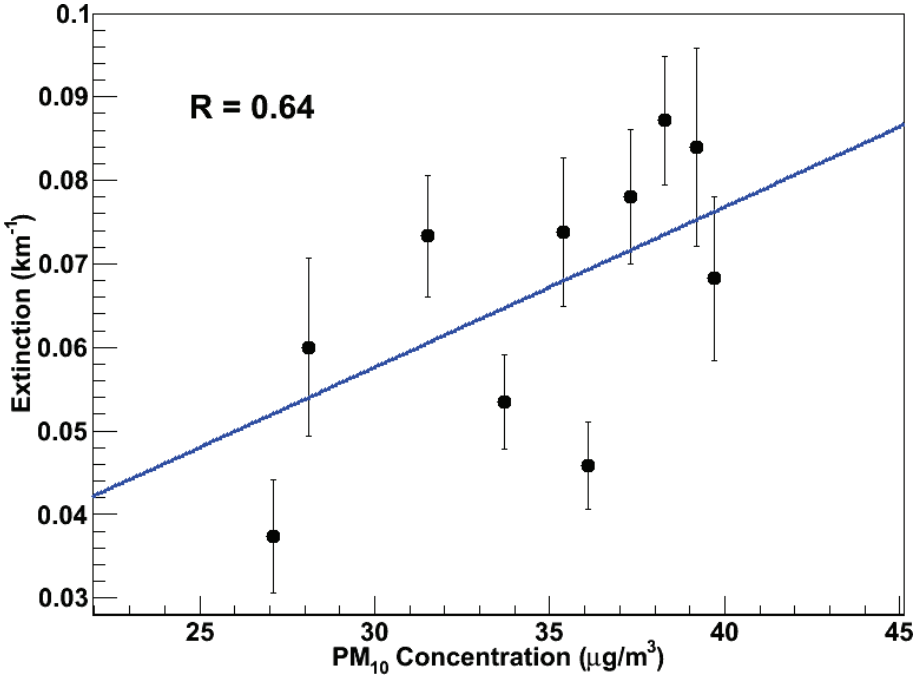

Fig. 8. The correlation between the lidar derived horizontal atmospheric extinction (α) and PM_{10} concentration (c) was found to be linear, $\alpha = (0.00192 \pm 0.00012)c$, with a correlation coefficient of 0.64. In the fit, α was constrained to zero for the limit case when PM_{10} concentration is zero.

AMTD
4, 6387–6410, 2011